CORRELATION OF A TWO-PHASE MODEL FOR MACRORETICULAR RESIN CATALYST IN SUCROSE INVERSION

SON-KI IHM AND IN-HWAN OH

Department of Chemical Engineering, Korea Advanced Institute of Science and Technology, Seoul, Korea

Key Words: Chemical Reaction, Sucrose Inversion, Macroreticular Resin Catalyst, Batch Reactor, First Order Reaction, Pore Effectiveness Factor, Microparticle Effectiveness Factor, Active Acidic Site, Model

Sucrose inversion was carried out in a batch reactor, using two types of macroreticular resin catalyst (Amberlyst 15 and Amberlyst XN-1010). Experimental data were obtained to determine the effect of particle size, reaction temperature and resin amount on the initial reaction rates. A two-phase model, proposed by the authors, was applied to elucidate the interaction between reaction and diffusion inside the resin particle. The present reaction is of first order and the overall effectiveness factor can be expressed analytically in terms of the pore- and the microparticle effectiveness factors together with the fraction of active acidic sites exposed to the pore space. The experimental data were in excellent correlation with the proposed model.

Introduction

Most previous studies on sucrose inversion catalyzed by ion exchange resin in aqueous solutions have been carried out by using either batch or fixed-bed reactor. The most comprehensive work with the batch reactor was reported by Bodamer and Kunin,[2] who measured the inversion rate for varying particle size, porosity and temperature. Wadman[20] also carried out hydrolysis of certain sugar glycosides such as maltose, sucrose and starch in a batch reactor. Many works dealing with the fixed-bed reactor have been reported in past years. Reed and Dranoff[15] studied the kinetics of continuous sucrose inversion catalyzed over a fixed bed of ion exchange resins in acid form. Lifshuts and Dranoff[11] studied the inversion of concentrated sucrose solution containing up to 45 wt% sucrose at temperature near 60°C by using fixed beds of resin catalysts. McGovern and Dranoff[13] also studied the inversion of sucrose by partially deactivated ion exchange resin catalyst in a fixed-bed reactor under conditions where intraparticle diffusion of sucrose was slow.

The first theoretical study on the kinetics of sucrose inversion catalyzed by a cation exchange resin was performed by Gilliland *et al.*,[4] who investigated the reaction as a function of temperature and particle size. The Wheeler–Thiele model for simultaneous diffusion and reaction was used to correlate the experimental data in the gelular resin particle to find the diffusivity and the intrinsic reaction rate constant.

In the present work, the liquid-phase sucrose inversion reaction, performed in a batch reactor by using two types of macroreticular ion exchange resins, was investigated to understand the effects of particle size, reaction temperature and resin amount. The parameters concerning intraparticle diffusion and reaction were obtained by correlating with the two-phase model which the authors have proposed.[7]

1. Theoretical Consideration

Macroreticular resins consist of agglomerates of very small randomly packed gelular microparticles with continuous nongel pores. Reactants may move more easily into the interior of the macroreticular resin bead through these large pores than gelular resins which have a continuous microporous matrix throughout. Macroreticular ion exchange resins might be analyzed as a bidisperse pore structure of micro- and macropores by taking the microparticles as having micropores. The pore structure and the properties of the macroreticular ion exchange resins are reported in the literature[8-10] and modeling of macroreticular ion exchange resins has been done by several authors.[3,18]

Two different kinds of active sites exist in the microsphere of macroreticular resin.[7,12,16] A fraction γ of the total active sites are located on the surface of the microparticle and provide easy access to the reactants. However, the remaining functional groups of fraction $1-\gamma$ are located within the polymer matrix of the microparticle. Molecules from the external

Received September 24, 1982. Correspondence concerning this article should be addressed to S. K. Ihm.

phase must penetrate through the polymer matrix in order to gain access to the inner active functional groups. For the sake of simplicity, it is assumed that the active sites of the functional groups are uniformly distributed over the pore walls (surface of the microsphere) and also in the gelular microsphere, hence that reaction occurs on the pore walls as well as in the gelular microspheres.

If the time of concentration change in the solution is large compared to the average residence time of a reactant molecule in the resin, the resin particle can be safely assumed to be in a quasi-steady state.[1,6] It is also assumed that there is no resistance to mass transfer at the catalyst surface. Under these assumptions, governing equations can be written for the first-order irreversible reaction in a batch reactor which contains W grams of catalyst with density ρ and V cubic centimeters of solution with concentration C as follows.

microsphere: $$\frac{D_i}{r_i^2}\frac{d}{dr_i}\left(r_i^2\frac{dC_i}{dr_i}\right)=\frac{(1-\gamma)e}{nV_i}kC_i \tag{1}$$

resin particle:

$$\frac{\varepsilon D_a}{r_a^2}\frac{d}{dr_a}\left(r_a^2\frac{dC_a}{dr_a}\right)=\frac{\gamma e}{V_a}kC_a+\frac{3(1-\varepsilon)}{R_i}D_i\left(\frac{dC_i}{dr_i}\right)_{r_i=R_i} \tag{2}$$

reactor: $$-V\frac{dC}{dt}=\frac{3\varepsilon D_a}{R_a}\frac{W}{\rho}\left(\frac{dC_a}{dr_a}\right)_{r_a=R_a} \tag{3}$$

and the initial and boundary conditions are

$$t=0;\quad C_i=C_a=0,\quad C=C_o \tag{4}$$

$$t>0;\quad r_i=R_i,\quad C_i=C_a;\quad r_i=0,\quad \frac{dC_i}{dr_i}=0 \tag{5-1}$$

$$r_a=R_a,\quad C_a=C;\quad r_a=0,\quad \frac{dC_a}{dr_a}=0 \tag{5-2}$$

Equations (1) and (2) can easily be solved with the boundary conditions[7]

$$C_i=\frac{R_iC_a}{r_i}\frac{\sinh\frac{r_i}{R_i}m_i}{\sinh m_i} \tag{6}$$

$$C_a=\frac{R_aC}{r_a}\frac{\sinh\frac{r_a}{R_a}M}{\sinh M} \tag{7}$$

where

$$m_i=R_i\sqrt{\frac{(1-\gamma)ek}{nV_iD_i}}=R_i\sqrt{\frac{(1-\gamma)e'k\rho}{(1-\varepsilon)D_i}} \tag{8}$$

$$M=R_a\sqrt{\frac{ek\{\gamma+(1-\gamma)\eta_i\}}{\varepsilon V_aD_a}}=R_a\sqrt{\frac{e'k\rho}{\varepsilon D_a}\{\gamma+(1-\gamma)\eta_i\}} \tag{9}$$

and

$$\eta_i=\frac{3}{m_i}\left(\frac{1}{\tanh m_i}-\frac{1}{m_i}\right) \tag{10}$$

With this solution, Eq. (3) becomes

$$-\frac{dC}{dt}=\bar{k}C \tag{11}$$

where

$$\bar{k}=\frac{3\varepsilon D_aW}{R_a^2V\rho}\left(\frac{M}{\tanh M}-1\right) \tag{12}$$

Integrating Eq. (11) results in the following expression of the overall first-order kinetics,

$$\ln\frac{C}{C_o}=-\bar{k}t \tag{13}$$

Equation (11) can be also written in terms of the overall effectiveness factor η_{ov} as

$$-\frac{dC}{dt}=\frac{We'kC}{V}\eta_{ov} \tag{14}$$

where

$$\eta_{ov}=\{\gamma+(1-\gamma)\eta_i\}\eta_a \tag{15}$$ [7,14]

$$\eta_a=\frac{3}{M}\left(\frac{1}{\tanh M}-\frac{1}{M}\right) \tag{16}$$

The value of an apparent overall reaction rate constant, $\bar{k}$, in Eq. (11) will vary with catalyst concentration; therefore the overall reaction rate equation based on the equivalents of the catalyst used is preferred as follows:

$$r_{ov}=-\frac{1}{We'}\frac{d(VC)}{dt}=\frac{\bar{k}}{We'}(VC)$$

$$=kC\eta_{ov}=\frac{3\varepsilon D_aC}{e'\rho R_a^2}\left(\frac{M}{\tanh M}-1\right) \tag{17}$$

Substituting C_o for C in the Eq. (17) the initial overall reaction rate is obtained as

$$r_o=\frac{\bar{k}}{We'}VC_o=kC_o\eta_{ov} \tag{18}$$

Experimental Techniques

The reactor consisted of a Pyrex glass 4-neck flask (1000 ml) with a condenser and a thermometer, and it was immersed in a water bath. To eliminate mass transfer resistance at the catalyst surface, a mechanical sleeve stirrer with a speed controller was used. For continuous analysis of the reaction, a polarimeter tube was placed in the circulation loop. This polarimeter set of tube, pump, and circulating line was wrapped with heating tapes and the temperature was controlled by means of a temperature controller. The entrance to the pump was covered with screen to prevent any of the resin catalyst beads from entering into the circulation line.

The resins used as catalyst were supplying by Rohm & Haas Co. Two kinds of resins were used in the

Table 1. Properties of resins

Properties	Amberlyst 15	Amberlyst XN-1010
Weight capacity of dry resin (meq/g)	4.50	3.30
% of surface–SO_3H groups ($\gamma \times 100$)	4.39	52.78
Internal surface area (m^2/g)	55	540
Porosity vol (%)	36	50
Avg. pore diameter (Å)	265	51
Cross-linkage (%)	20–25	*

* No data on cross-linkage of Amberlyst XN-1010 are available, but it may be higher than that of Amberlyst 15, comparing the other properties.

experiments: Amberlyst 15 and Amberlyst XN-1010. The properties of the resin catalysts are listed in **Table 1**. The acid form resins were separated into several size fractions by wet-screening with standard sieves. The screening process was repeated twice under a stream of distilled water to ensure good classification, and the broken beads were removed by rolling them on an inclined flat plate.

A volume of 300–500 ml of sucrose solution with concentration of 0.2 g/ml (0.5843 M) were introduced into a reactor, and were heated to a desired temperature under the stirred condition. The recirculation rate was made fast enough such that the residence time in the recirculating line was very short and no appreciable temperature difference could be detected. When the temperature of the sucrose solution reached the desired value, preconditioned resin catalysts were introduced into the reactant solution and polarimetric readings were taken every ten minutes to cover the initial stage of the reaction. The reaction was followed by observing the optical power of solution as a function of time using a polarimeter (Polyscience Corp. Model SR 6). Data were obtained for different values of particle sizes, reaction temperatures and resin amounts.

Results and Discussion

In all experiments the fraction of the sucrose unconverted could be calculated from measurements of the optical rotation of reaction solution, assuming that the sucrose was hydrolyzed to form equal amounts of fructose and glucose. One may safely neglect the mutarotation reaction between α- and β-form because the mutarotation reaction is much faster than the inversion reaction. The equilibrium state between α- and β-form is reached as soon as the sucrose is converted to the products. Plotting of the logarithmic mole fraction of unconverted sucrose versus the time results in a straight line if the apparent reaction is of first-order as shown in Eq. (13). Apparent overall reaction rate constant, $\bar{k}$, can be calculated from the slope of such lines, and is related

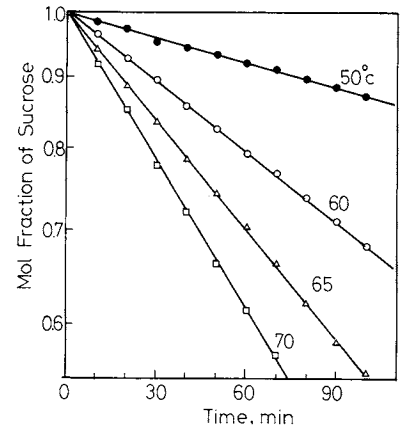

Fig. 1. Sucrose inversion by Amberlyst XN-1010 showing effects of temperature at a particle size of 32–50 mesh (6.15 g).

to parameters such as the intrinsic reaction rate constant, the microdiffusivity and the pore diffusivity through Eq. (12). **Figure 1** shows typical straight lines obtained for sucrose inversion by Amberlyst XN-1010 at 50, 60, 65 and 70°C, respectively. In view of this linearity, the present modeling and the quasi-steady state assumption seem to be reasonable in our experiments. Other investigators[2,4] also have found that hydrolysis of sucrose catalyzed by cation exchange resins was a first-order reaction. **Table 2** summarizes the effect of temperature and particle size for the two kinds of catalysts in terms of the initial overall reaction rates, which are in turn calculated from the apparent overall reaction rate constant. The results show more rapid inversion with smaller size particles and at higher reaction temperature, as expected.

The temperature dependence of the initial overall reaction rates from Table 2 could be explained by the Arrhenius plot shown in **Fig. 2**. The data do not follow the usual Arrhenius equation but deviate downward from the straight lines at higher temperatures; similar tendencies appear in the literature.[5,19] This drop in activation energy of the reaction with increased temperature is mainly due to the fact that the reaction rate is related not only to the reaction constants but also to the diffusivity. As the temperature increases, reaction becomes so rapid compared to diffusion that the reactant reacts before it can diffuse into the resin catalyst, and therefore all of the active sites in the resin are not being effectively used. This diffusion limitation becomes more serious at larger particle size as well as at higher temperature as shown in Fig. 2. Analysis of such data requires isolation of the reaction and the diffusion from the overall process.

Some studies,[4,11,15] however, show that the experimental data of the apparent reaction rate constants (or initial overall reaction rates) conform well to such an Arrhenius plot over a considerable range of tem-

Table 2. Tabulation of experimental data for sucrose inversion on resins

Species	T [°C]	R_a [cm]	$r_o \times 10^2$ [mol/min·eq]	M	$k \times 10^3$ [cm³/s·meq]	η_i	η_a from Eq. (18)	η_{ov}
Amberlyst 15								
	50	0.02	0.80	0.65	0.68	0.32	0.95	0.34
		0.0328	0.77	1.06			0.92	0.32
		0.0428	0.76	1.38			0.90	0.32
	60	0.02	2.74	1.21	1.89	0.42	0.92	0.41
		0.0328	2.35	1.98			0.79	0.36
		0.0428	2.13	2.59			0.71	0.32
	70	0.02	6.78	1.88	4.23	0.51	0.87	0.46
		0.0328	5.61	3.07			0.72	0.38
		0.0428	4.28	4.01			0.55	0.29
		0.0545	3.69	5.11			0.47	0.25
Amberlyst XN-1010								
	50	0.02	1.23	0.34	0.68	0	0.98	0.52
		0.0328	1.23	0.55			0.98	0.52
		0.0428	1.22	0.72			0.97	0.51
		0.065	1.17	1.10			0.93	0.49
	60	0.02	3.44	0.53	1.89	0	0.98	0.52
		0.0328	3.34	0.87			0.96	0.50
		0.0428	3.26	1.13			0.93	0.49
		0.065	2.96	1.72			0.85	0.45
	65	0.02	5.37	0.64	2.97	0	0.98	0.52
		0.0328	5.06	1.04			0.92	0.49
		0.0428	5.06	1.36			0.92	0.49
		0.065	4.33	2.07			0.97	0.42
	70	0.02	7.59	0.69	4.23	0	0.97	0.51
		0.0328	7.15	1.13			0.91	0.48
		0.0428	6.84	1.47			0.87	0.46
		0.065	6.14	2.24			0.78	0.41

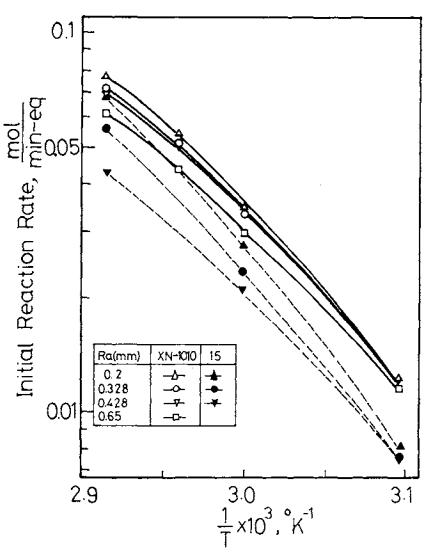

Fig. 2. Temperature dependence on initial reaction rates at various particle sizes.

peratures with an activation energy of 16–18 kcal per mol. This seems to be due to the fact that the catalysts used in their experiments were not macroreticular resin catalysts but gelular ones, the three-dimensional polymeric matrix of which was homogeneous structure with no discontinuities. Catalysis of the liquid-phase reactions by such a gelular ion exchange resin may not be similar to heterogeneous catalysis, but may be described more adequately as quasihomogeneous catalysis because the sulfonic acid group bound to the polymer matrix will be dissociated into a polyanion and a proton with the electrostatic interaction between them in a hydrated state.

Experiments made at 70°C with various amounts of Amberlyst 15 show that the apparent reaction rate constants increase with resin amount. But the initial reaction rates based on the equivalents of the resins were nearly constant regardless of the amounts of resin catalysts used in this experiment.

Comparing the two resin catalysts, Amberlyst 15 was observed to be slightly less effective than Amberlyst XN-1010. Although the capacity of Amberlyst 15 is larger than that of Amberlyst XN-1010, reaction which occurred near the pore walls of Amberlyst 15 must be much less than that of Amberlyst XN-1010 due to the much smaller value of γ. All of the active sites in Amberlyst 15 are less effectively used than in Amberlyst XN-1010, hence the initial reaction rates of Amberlyst 15 become less than those of XN-1010.

Parameter Estimation

The true chemical reaction rate constant, k, the microdiffusivity, D_i, and the pore diffusivity, D_a, are not known but they can be assumed to be constant and independent of the resin particle sizes at a

specified reaction temperature. Therefore the microsphere Thiele modulus, m_i, which is a function of k, D_i, and the radius R_i of the microsphere, can be assumed to be constant for a specific resin species because the radius R_i of the microsphere within the particle is of uniform size as is usually confirmed by scanning electron microscopy.

Hence from Eq. (9), the ratio of the modified Thiele modulus is

$$\frac{M_1}{M_2}=\frac{R_{a_1}}{R_{a_2}} \tag{19}$$

On the other hand, the ratio of the effectiveness factor (or the initial overall reaction rate) is

$$\frac{r_{o_1}}{r_{o_2}}=\frac{\dfrac{1}{{M_1}^2}\left(\dfrac{M_1}{\tanh M_1}-1\right)}{\dfrac{1}{{M_2}^2}\left(\dfrac{M_2}{\tanh M_2}-1\right)}=\left(\frac{R_{a_2}}{R_{a_1}}\right)^2\frac{\dfrac{M_1}{\tanh M_1}-1}{\dfrac{M_2}{\tanh M_2}-1} \tag{20}$$

Now M_1 and M_2 can be found by solving Eqs. (19) and (20) simultaneously because r_{o_1} and r_{o_2} are measured for the given values of R_{a_1} and R_{a_2}. With this modified Thiele modulus at the specific temperature the pore diffusivity, D_a, can be found from Eq. (12):

$$D_a=\frac{V\rho {R_a}^2\bar{k}}{3W\varepsilon\left(\dfrac{M}{\tanh M}-1\right)} \tag{21}$$

and accordingly the apparent reaction rate constant, k_{app}, which lumps the intrinsic reaction rate, k, and the microdiffusivity, D_i, can be found from Eq. (9):

$$k_{\text{app}}=k\{\gamma+(1-\gamma)\eta_i\}=\frac{M^2\varepsilon D_a}{{R_a}^2 e'\rho} \tag{22}$$

By taking the values of r_{o_1} and r_{o_2} for all possible combinations of two particle diameters R_{a_1} and R_{a_2} from the experimental data, one can obtain as many estimations for D_a and k_{app} as the number of combinations. From these estimations, the values of the parameters were calculated by the nonlinear least squares method giving the least of the error sums. The parameters at various reaction temperatures were calculated from the experimental data by the nonlinear least squares method,[14] and are shown in **Figs. 3** and **4**. From the values of the pore diffusivity, D_a, in Fig. 3, the activation energy of diffusion can be obtained; 1.04 kcal/mol for Amberlyst 15 and 4.01 kcal/mol for Amberlyst XN-1010. From the pore diffusivity and the activation energy of diffusion we can anticipate that although the average pore of Amberlyst 15 is larger than that of XN-1010, the swelling effect from a dry state to a water-saturated state of Amberlyst 15 (the swelling percentage is 66%)[17] makes the pores shrink so closely that the diffusivity for Amberlyst 15 becomes smaller than that for Amberlyst XN-1010, also that the activation

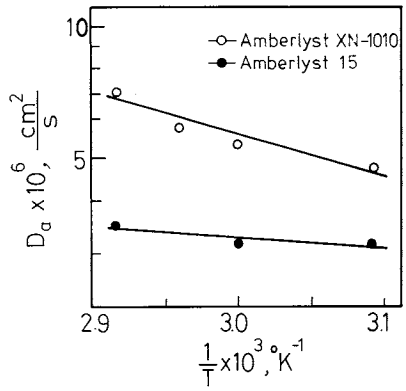

Fig. 3. Arrhenius plot of the pore diffusivity.

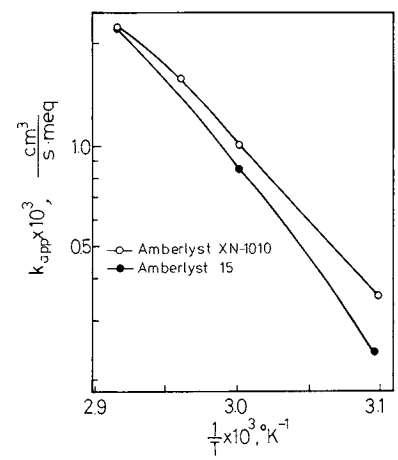

Fig. 4. Arrhenius plot of apparent reaction rate constant.

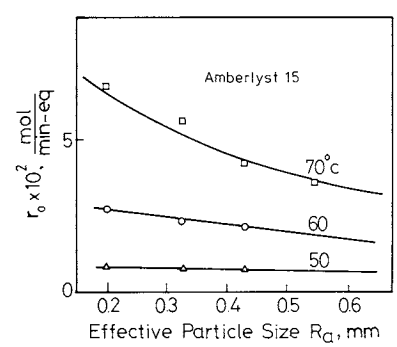

Fig. 5. Correlation of experimental results for Amberlyst 15.

energy for Amberlyst 15 becomes smaller than that for Amberlyst XN-1010.

Figures 5 and **6** show the relation between the initial overall reaction rate and particle size for Amberlyst 15 and for XN-1010 respectively, using the estimated parameters. The effect of particle size on Amberlyst 15 is slightly stronger than that on Amberlyst XN-1010 as the temperature increases due to the increased diffusion limitations as previously discussed.

On the other hand, if the microdiffusivity and the intrinsic reaction rate constant can be calculated independently of the apparent reaction rate constant, $k_{\text{app}}=k\{\gamma+(1-\gamma)\eta_i\}$, the overall effectiveness factor

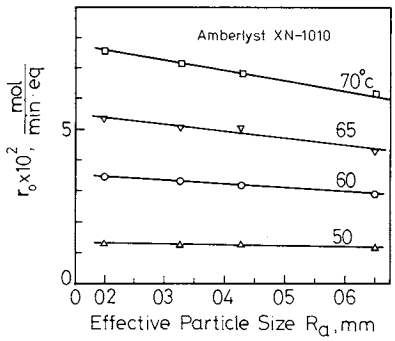

Fig. 6. Correlation of experimental results for Amberlyst XN-1010.

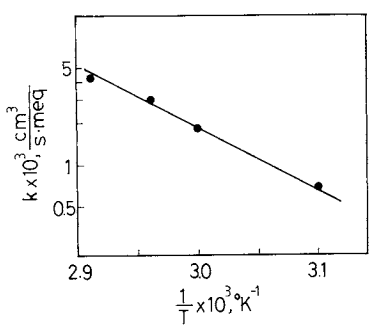

Fig. 7. Arrhenius plot of intrinsic reaction rate constants for Amberlyst XN-1010.

can be found by Eq. (18), and can be compared with the theoretical values calculated from Eq. (15).

For Amberlyst XN-1010 the fraction of the total active sites distributed over the surface of the microparticle (the pore wall) is about 0.5278, hence it can be assumed that reaction occurs mostly on the pore walls before the reactant molecules penetrate through the microparticles. Moreover, higher cross-linkage of Amberlyst XN-1010 must suppress the penetration of the molecules. With this condition the microeffectiveness factor, η_i, can be assumed to be zero, and the intrinsic reaction rate constant can be estimated at a given temperature from Eq. (22). **Figure 7** shows the Arrhenius plot of the estimated intrinsic reaction rate constant, from which the activation energy of reaction is found to be 20.1 kcal/mol.

Now with another assumption that the intrinsic reaction rate constant for Amberlyst 15, with a γ value of 0.0439, (that is, most of the active sites are not located on the pore walls but in the gelular microparticles), is equal to that for Amberlyst XN-1010, the microeffectiveness factor, η_i, can be calculated from the relation of $k_{app}=k\{\gamma+(1-\gamma)\eta_i\}$. The microdiffusivity, D_i, can be calculated in turn from η_i, and is shown in the Arrhenius plot of **Fig. 8**. From the slope in Fig. 8, the activation energy of diffusion through the gelular microparticle of Amberlyst 15 is found to be 32.4 kcal/mol.

Using the estimated parameters, the effectiveness factors can be calculated, and are also tabulated in

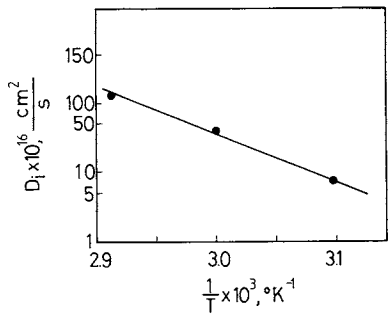

Fig. 8. Arrhenius plot of microdiffusivities for Amberlyst 15.

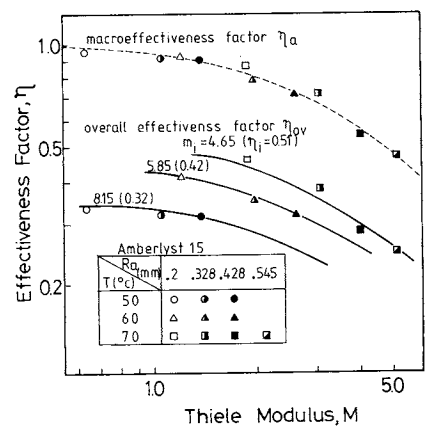

Fig. 9. Effectiveness factors for Amberlyst 15.

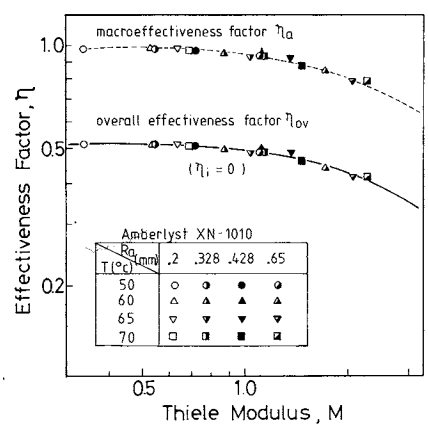

Fig. 10. Effectiveness factors for Amberlyst XN-1010.

Table 2. **Figures 9** and **10** show good agreement between the theoretical effectiveness factors and the experimental ones. The macroeffectiveness factors decrease as particle size and temperature increase for both resins.

Figure 9 shows that with Amberlyst 15 the microeffectiveness factor increases as temperature increases. This is because the swellability of the gelular microparticle is increased with temperature. It is rather interesting that the overall effectiveness factor tends to increase with reaction temperature for a smaller resin particle (say $R_a=0.2$ mm) with negligible resistance to pore diffusion (i.e., $\eta_a \approx 1$). As particle size

increases, however, pore diffusion is more controlling and the increased swellability of the polymeric matrix will be offset by the increased diffusion limitation in the pore space. It can be seen that for a larger particle (say $R_a > 0.428$ mm) the overall effectiveness factor does not increase but tends to decrease with temperature.

In Fig. 10 for the case with Amberlyst XN-1010, it is shown that the behavior of the overall effectiveness factor is the same as that of the macroeffectiveness factor since the microparticle is inert (i.e., $\eta_i = 0$).

Acknowledgment

This work was presented at 32nd Canadian Society of Chemical Engineering Conference, October 4–6, 1982, Vancouver. The authors acknowledge the valuable comments from Mr. Sung-Sup Suh in revising this paper.

Nomenclature

C	=	concentration	[mol/cm^3]
D	=	effective diffusivity	[cm^2/s]
e	=	weight capacity of a resin particle with volume V_a	[eq]
e'	=	weight capacity of a resin particle, $e(1-\varepsilon)/nV_i\rho$ or $e/v_a\rho$	[eq/g]
k	=	intrinsic reaction rate constant based on equivalent; k_{app}, apparent reaction rate constant, defined by Eq. (22)	[cm^3/s·meq]
$\bar{k}$	=	overall reaction rate constant	[l/min]
M	=	Thiele modulus, defined by Eq. (9)	
m_i	=	Thiele modulus, defined by Eq. (8)	
n	=	number of microspheres involved in a resin particle	
R	=	radius	[cm]
r	=	radial position from the center	[cm]
r_{ov}	=	overall reaction rate based on the equivalent of the catalyst; r_o, initial overall reaction rate	[mol/min·eq]
t	=	time	[min]
V	=	volume	[cm^3]
W	=	catalyst weight	[g]
γ	=	fraction of active sites distributed on the surface of the microsphere	
ε	=	porosity	
η	=	effectiveness factor	
ρ	=	apparent density of the resin	[g/cm^3]

〈Subscript〉

a	=	resin particle
i	=	microsphere
o	=	initial

Literature Cited

1) Almeida, J. Jr. and D. Glasser: *South Africa J. Sci.*, **69**, 109 (1973).
2) Bodamer, G. and R. Kunin: *I & EC*, **43**, 1082 (1951).
3) Frisch, N. W.: *CES*, **17**, 735 (1962).
4) Gilliland, E. R., H. J. Bixler and J. E. O'Connell: *I & EC, Fundm.*, **10**, 185 (1971).
5) Gupta, V. P. and W. J. M. Douglas: *AIChE J.*, **13**, 883 (1967).
6) Helfferich, F.: "Ion Exchange," McGraw-Hill, New York (1962).
7) Ihm, S. K., S. S. Suh and I. H. Oh: *J. Chem. Eng. Japan*, **15**, 206 (1982).
8) Kun, K. A. and R. Kunin: *J. Polymer Sci., C*, **16**, 1457 (1967).
9) Kunin, R., E. Meitzner and N. Bortnick: *J. Am. Chem. Soc.*, **20**, 305 (1962).
10) Kunin, R., E. Meitzner, J. A. Oline, S. A. Fisher and N. Frisch: *I & EC, Prod. Res. and Dev.*, **1**, 140 (1962).
11) Lifshuts, N. and J. S. Dranoff: *I & EC, Process Des. & Dev.*, **7**, 267 (1968).
12) Martinek, A., K. Setinek and L. Bernek: *J. Catalysis*, **51**, 86 (1978).
13) McGovern, T. J. and J. S. Dranoff, *AIChE J.*, **16**, 536 (1970).
14) Oh, I. H.: M.S. Thesis, Korea Advanced Institute of Science and Technology (1981).
15) Reed, E. W. and J. S. Dranoff: *I & EC, Fundm.*, **3**, 304 (1964).
16) Rodriguez, O. and K. Setinek: *J. Catalysis*, **39**, 449 (1975).
17) Rohm & Hass Co.: "Amberlyst 15," Philadelphia (1972).
18) Ruckenstein, E., A. S. Vaidyanathan and G. R. Youngquist: *CES*, **26**, 1305 (1971).
19) Suh, S. S. and S. K. Ihm: *J. Korean Inst. Chem. Eng.*, **18**, 461 (1980).
20) Wadman, W. H.: *J. Chem. Soc.*, 3051 (1952).